nature materials

ARTICLES

PUBLISHED ONLINE: 29 NOVEMBER 2009 | DOI: 10.1038/NMAT2584

Exceptional high-temperature stability through distillation-like self-stabilization in bimetallic nanoparticles

Anmin Cao[1,2] and Götz Veser[1,2]*

Metal nanoparticles with precisely controlled size and composition are highly attractive for heterogeneous catalysis. However, their poor thermal stability remains a major hurdle on the way towards application at realistic technical conditions. Recent progress in this area has focused on nanostructured oxides to stabilize embedded metal nanoparticles. Here, we report an alternative approach that relies on synthesizing bimetallic nanoparticles with precise compositional control to obtain improved high-temperature stability. We find that PtRh nanoparticles with sufficiently high Rh content survive extended calcination at temperatures up to ∼850 °C without significant sintering. For lower Rh content, sacrificial self-stabilization of individual nanoparticles through a distillation-like process is observed: the low-melting-point metal (Pt) bleeds out and the increasing concentration of the high-melting-point metal (Rh) leads to re-stabilization of the remaining nanoparticle. This principle of thermal self-stabilization should be broadly applicable to the development of multi-metallic nanomaterials for a broad range of high-temperature applications.

The advantages of nanosized particles in heterogeneous catalysis have long been recognized[1–3]. The increasing dispersion, that is, increasing surface-to-volume ratio, with decreasing particle size strongly increases the specific catalytic activity, and quantum confinement effects can completely alter the chemical characteristics of sufficiently small nanoparticles[4–6]. Furthermore, the atomic characteristics of metallic nanoparticles, including particle size and surface composition, have been shown to be critical to catalytic activity and selectivity[7–10]. In particular, the rapid advances in colloid chemistry over the past decade have resulted in the synthesis of nanocatalysts with tunable size, shape and composition, which have been used as model catalytic systems to investigate synthesis–structure–activity correlations in nanocatalysts[10–12].

However, an inherent problem for nanocatalysts is their well-documented lack of stability at realistic technical conditions[4,13–15]. Supported and unsupported metal nanoparticles show rapid growth at reactive conditions especially if the reaction temperature is very high[4,13]. For many industrially important catalytic processes, such as catalytic combustion, steam reforming and automobile-exhaust control, reaction temperatures are typically in excess of 600 °C, and thermal stability of the catalyst becomes a crucial issue[16–18]. Organic capping agents, which are widely used in colloidal chemistry to stabilize nanoparticles at mild conditions, decompose at temperatures above ∼300–400 °C, leaving the uncapped nanoparticles unprotected against sintering and deactivation[13,14].

Control and stabilization of metal nanoparticles is a particularly critical issue in the size range below ∼5 nm, that is, in the so-called 'mitohedrical' region in which pronounced nanosize effects are found[19,20]. A recent strategy, in which Pt nanoparticles were encapsulated in a porous silica shell, shows promising results for high-temperature stabilization of nanocatalysts, but has so far been demonstrated only for comparatively large nanoparticles (∼10–15 nm; ref. 13). Similarly, our own previously developed strategy of stabilizing metal nanoparticles by means of embedding them into nanostructured oxides is limited at high temperatures to particle sizes above 10 nm (ref. 21). So far, no efficient approach to stabilizing particles in the mitohedrical region has been proven.

Compared with the widespread investigation of organic materials and metal oxides as stabilizing matrices for metal nanoparticles[14,22], the effect of varying the composition of metal nanoparticles through alloying on thermal stability has found very little attention. Whereas bimetallic nanocatalysts, composed of two different metal elements, are the focus of intense research efforts in catalysis[11,23], the thermal stability of bimetallic nanoparticles has not been studied in detail, and, despite its importance for technical application of nanocatalysts, the evolution of single bimetallic nanoparticles at high-temperature conditions has so far not been given much attention.

Here, we demonstrate the possibility to synthesize PtRh nanoparticles with exceptional thermal stability by using the impact of alloying Pt with Rh on thermal stability. Bimetallic PtRh–BHA nanocomposites (BHA: barium hexa-aluminate, a high-temperature-stabilized alumina with a crystallization temperature around 1,200 °C) are prepared in a straightforward and efficient one-pot synthesis[21], which results in PtRh nanoparticles with a narrow size distribution around 4 nm, homogeneously dispersed throughout the BHA support. Most importantly, the bimetallic nanoparticles show exceptional thermal stability, surviving extended high-temperature calcination at temperatures up to 850 °C without significant changes in their particle-size distribution. Interestingly, this stability is a sensitive function of the Pt/Rh ratio. Phase separation is observed for the PtRh nanoparticles at high temperature: Pt bleeds out and the increasing Rh content in the remaining PtRh nanoparticle leads to the re-stabilization of the nanoparticle. This process happens continuously as a function of temperature, similar to the operation of a distillation process, gradually bleeding

---

[1] National Energy Technology Laboratory, US Department of Energy, PO Box 10940, Pittsburgh, Pennsylvania 15236, USA, [2] Department of Chemical Engineering, University of Pittsburgh, Pittsburgh, Pennsylvania 15261, USA. *e-mail: gveser@pitt.edu.

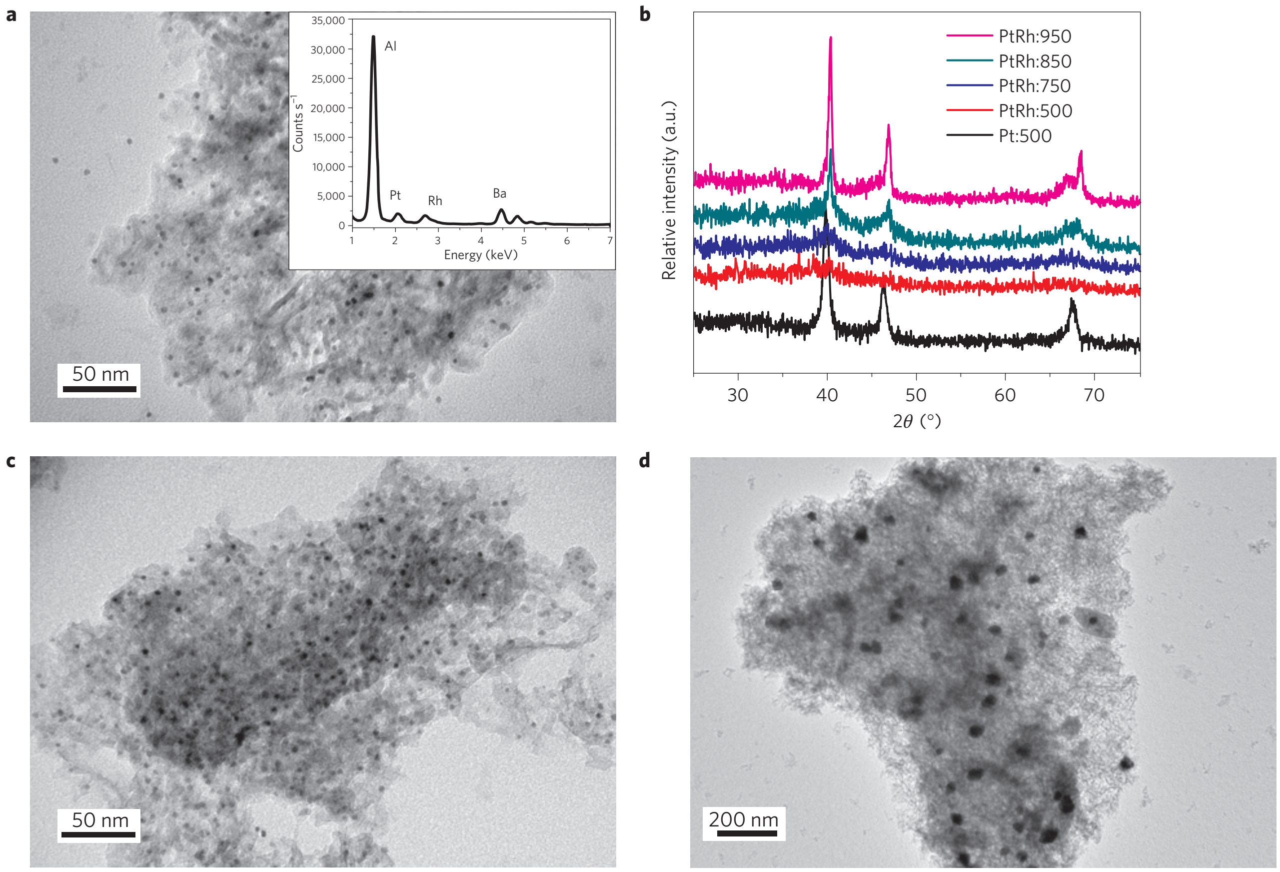

Figure 1 | TEM and XRD characterizations of PtRh (1:1)–BHA calcined at different temperatures. a, TEM image for PtRh–BHA calcined at 500 °C (inset: EDAX pattern). **b**, XRD patterns for PtRh–BHA calcined at different temperatures. **c**,**d**, TEM images for PtRh–BHA calcined in air at 850 °C (**c**) and 950 °C (**d**) for 2h.

Pt from the bimetallic nanoparticle, which stabilizes itself in this way. These PtRh nanocatalysts are furthermore shown to be highly active combustion catalysts with ignition temperatures for methane combustion (1% CH_4 in air) as low as 450 °C and complete conversion at 580 °C. As expected from the thermal stability, the catalyst is stable in successive ignition–extinction cycles, in contrast to monometallic Pt catalysts, which show lower activity and significant deactivation over several cycles.

Figure 1a shows a typical transmission electron microscope (TEM) image for a PtRh–BHA sample with an atomic ratio of Pt/Rh = 1:1(Pt: 5.3 wt%, Rh: 2.8 wt%). After calcination at 500 °C for 2 h, the sample shows the characteristics of a favourable catalytic nanoarchitecture with metal nanoparticles uniformly dispersed throughout the porous support. The metal nanoparticles show a narrow particle-size distribution with an average particle size of 4.1 ± 0.5 nm (Supplementary Fig. S1). Brunauer–Emmett–Teller measurements confirm a high specific surface area of 389.6 m^2 g^{-1} (Supplementary Fig. S2). The inset in Fig. 1a shows the energy-dispersive X-ray spectroscopy (EDAX) spectrum of the catalysts, demonstrating the coexistence of Pt and Rh. The Pt to Rh ratio is measured to be 50.7:49.3, which is in excellent agreement with the 1:1 ratio used for the synthesis. X-ray diffraction (XRD) characterization is carried out to further identify the bimetallic nanocatalysts. Surprisingly, for the sample calcined at 500 °C, no characteristic peaks can be observed (Fig. 1b). For comparison, monometallic Pt–BHA with the same amount of Pt is prepared by following the same synthetic protocol. For this pure Pt–BHA sample, the XRD patterns indicate well-crystallized Pt at the same temperature as indicated by the sharp peaks (bottom curve in Fig. 1b; JCPDS 87-0644). On further calcinations at increasingly high temperature, weak Pt reflexes finally become discernible at 850 °C and become sharper and more pronounced at 950 °C (Fig. 1b). This high temperature necessary for the formation of crystalline Pt is unexpected because Pt usually crystallizes at a much lower temperature. TEM images of the samples after calcination at 850 °C confirm an exceptional thermal stability of these samples. The metal nanoparticles remain essentially unchanged with an average diameter at 4.3 nm even after extended calcination at 850 °C (Fig. 1c). Only after calcination at 950 °C, bigger particles with average diameters of ~34 nm are observed (Fig. 1d). It is noteworthy, however, that although most of the PtRh particles have grown to ~34 nm size, careful investigation of a broad sample area in TEM still shows the presence of a small population of nanoparticles with diameters around 4 nm.

In the present synthesis, no special capping agents are used to stabilize the metal nanoparticles and the surfaces of the metal nanoparticles are free of any residual surfactant after the high-temperature calcinations. Furthermore, a blank experiment for Pt–BHA (Supplementary Fig. S3) shows that monometallic Pt nanoparticles sinter to ~20 nm at 600 °C, in good agreement with previous reports[21,24,25]. Pure Rh–BHA shows excellent thermal stability up to temperatures around 1,000 °C (Supplementary Information S1, Figs S4–S6), and a simple physical mixture of Pt–BHA and Rh–BHA shows, not surprisingly, that the thermal stability of individual Pt and Rh nanoparticles is unaffected by the presence of nanoparticles of the other respective metal in the mixture (Supplementary Information S2, Figs S7–S8). Clearly, the unusual thermal stability of PtRh–BHA, with nanoparticles <5 nm at 850 °C, is hence caused by the addition of a high-melting-point metal (Rh), resulting in the formation of highly stable

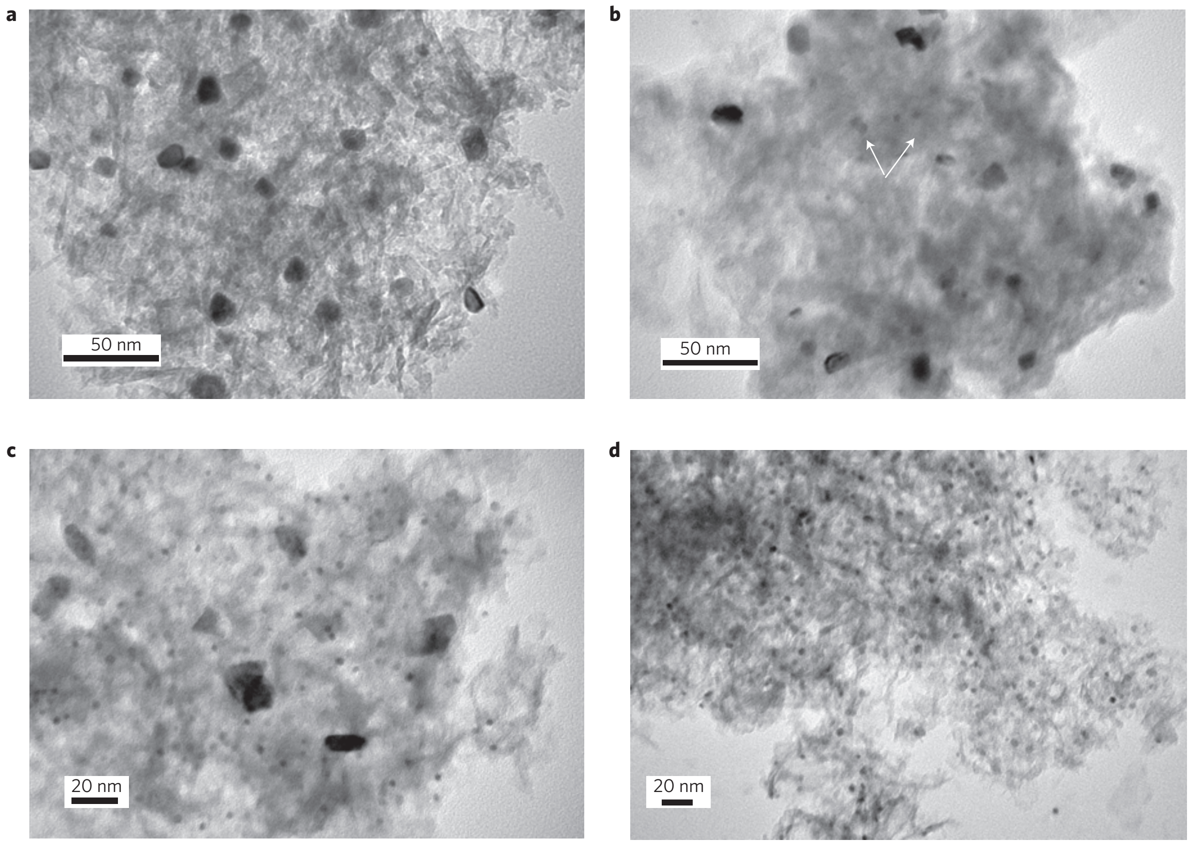

Figure 2 | TEM images of PtRh-BHAs calcined at 700 °C with different Pt/Rh ratios. a, 15:1. **b**, 5:1 (the white arrows indicate the emergence of small particles). **c**, 3:1. **d**, 1:1.

PtRh alloy nanoparticles. To the best of our knowledge, this is the first report of such exceptional high-temperature stability for metallic nanoparticles.

As Rh shows such a significant effect on the thermal stability of Pt nanoparticles, we further investigated the effect of the Pt/Rh ratio on particle stability. By controlling the amount of H_2PtCl_6 and $RhCl_3$ used in the synthesis, a series of PtRh–BHA nanocomposites were synthesized and calcined over a range of temperatures. Figure 2 shows typical TEM images of PtRh–BHA after calcination at 700 °C, with Pt/Rh ratios varying over a broad range: from 15:1, 5:1, 3:1 and 1:1 (Fig. 2a–d, respectively). For a PtRh–BHA sample with a very low Rh content (Pt/Rh = 15:1, Fig. 2a), the metal nanoparticles after calcination at 700 °C are large with a mean diameter around 23 nm. Increasing the Rh content to 5:1, we notice in addition to the large particles a few smaller particles emerging, as indicated by the white arrows in Fig. 2b. For a medium Pt/Rh ratio of 3:1, the smaller particles become dominant and only a few large particles exist in the sample, whereas for the 1:1 ratio, as mentioned above, the PtRh nanoparticles are highly stable with a uniform size distribution around 4 nm. Clearly, an increasing Rh content in the PtRh nanoparticles results in improved thermal stability. However, the transition from the stable particles at high Rh content to the less stable particles at low Rh content does not proceed continuously, but is characterized by two distinct size distributions at intermediate Pt/Rh ratios (Supplementary Fig. S9).

The mechanism through which Rh stabilizes the nanoparticles becomes apparent in further characterizations of the sample with an intermediate (3:1) ratio of Pt/Rh. After calcination at 600 °C, the PtRh nanoparticles are still uniformly small (Fig. 3a); that is, even at this reduced Rh content they show improved thermal stability over pure Pt particles. EDAX analysis confirms a Pt/Rh ratio of 74.6:26.4, in excellent agreement with the synthesis ratio of 3:1. After increasing the calcination temperature to 700 °C, larger particles with diameters around 20 nm emerge (Fig. 3b). Two representative particles were selected for further high-resolution TEM (HRTEM) characterization (white circle in Fig. 3b). The lattice fringes in the HRTEM image in Fig. 3c clearly show that both particles are highly crystalline. Figure 3d shows a fast Fourier transformation (FFT) analysis of the HRTEM image for the smaller particle. The inter-planar spacing is calculated to be 0.223 nm (Fig. 3d) and the two characteristic FFT points are in good agreement with diffraction from the (111) plane of PtRh alloy (JSPDS 27-0545). EDAX analysis (Fig. 3e) for the smaller particle further confirms that these particles contain both Pt and Rh, now with an atomic ratio at 69.2:31.8, that is, with a significant increase in Rh content over the original ratio of 3:1. In comparison, Fig. 3f shows the FFT pattern for the larger particle in Fig. 3c. The FFT pattern is characterized by hexagonal symmetry and is consistent with the typical diffraction pattern for fcc Pt (JSPDS 87-0644). In agreement with this, the EDAX analysis shows that the larger particles are pure Pt with no Rh signal detectable (Fig. 3g). A detailed EDAX analysis for a large population of nanoparticles at 600 and 700 °C, that is, at temperatures below and above the temperature where larger nanoparticles appear, further confirms a strong shift of the Pt/Rh ratio in the composition distribution of the smaller nanoparticles towards high Rh content owing to the loss of Pt (Fig. 4).

To further support the above observation and to test for the surface composition of the nanoparticles, CO adsorption/desorption was used as a chemical surface probe. The temperature-programmed desorption (TPD) spectrum of CO is widely used as a sensitive probe of CO–metal interactions in catalysts[26,27]. As shown in Fig. 5a, the desorption curve of Rh–BHA is broad with multiple peaks[28]. The desorption spectrum for pure

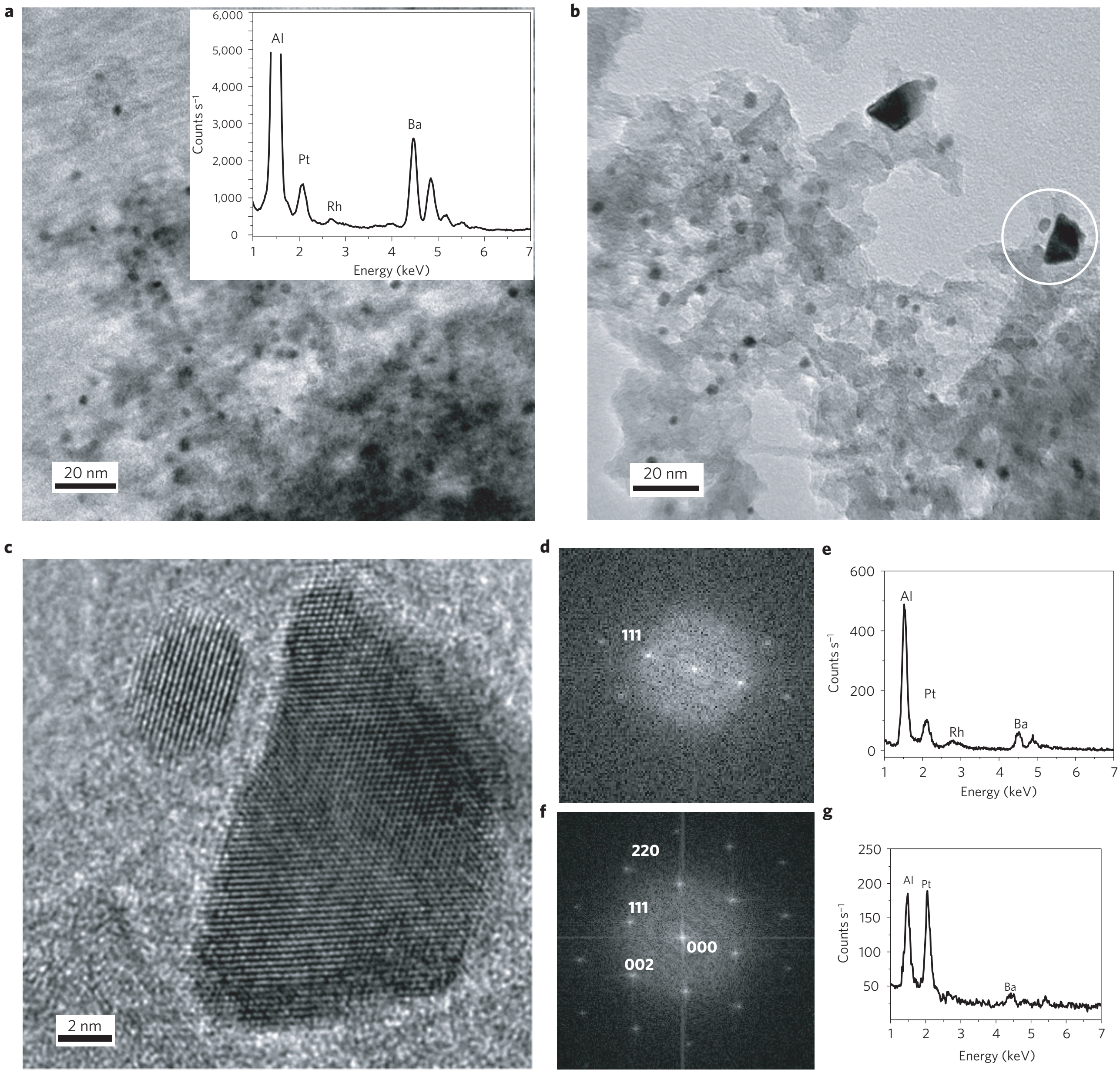

Figure 3 | TEM and EDAX characterization of PtRh–BHA (3:1). **a**, PtRh–BHA calcined at 600 °C (inset is its EDAX pattern). **b**, PtRh–BHA calcined at 700 °C. **c**, HRTEM image showing an enlarged view of the two representative small and large particles indicated by the white circle in **b**. **d**,**e**, The FFT pattern (**d**) and EDAX spectrum (**e**) for the smaller particle. **f**,**g**, The FFT pattern (**f**) and EDAX spectrum (**g**) for the larger particle.

Pt–BHA differs significantly from that, with only one pronounced peak centred around 390 °C. The CO TPD spectrum obtained for the PtRh–BHA calcined at 600 °C shows an intermediate peak between pure Pt and Rh, indicating the formation of an alloy phase[29]. However, after calcining the sample at 700 °C, the TPD spectrum is dominated by a new peak with a maximum at the same desorption temperature as for pure Pt–BHA, while still maintaining some of the broader background shoulders of the lower-temperature PtRh–BHA sample. The emergence of this new TPD peak is further confirmation that the 'new', larger particles formed on calcination at 700 °C are indeed pure Pt particles. At the same time, a population of small PtRh particles remains in the sample, as reflected in the broad shoulders. The result is further confirmed by XRD (Fig. 5b). After 600 °C calcination, the XRD pattern of the PtRh–BHA shows no distinct diffraction peaks, whereas the characteristic pattern for Pt emerges at 700 °C, identifying the newly formed particles as pure Pt (JSPDS 87-0644).

The sum of the above observations clearly indicates that the PtRh nanoparticles 'bleed out' Pt at high temperature, forming two populations of small, Rh-rich PtRh nanoparticles and larger, pure Pt nanoparticles. On the basis of these observations, we hence propose a 'distillation like' mechanism for the formation of Pt nanoparticles and the self-stabilization of the remaining PtRh nanoparticles by means of solid–liquid phase separation. As the detailed phase diagram for 4-nm nanoparticles is not known, we adapt the phase diagram for bulk PtRh (Supplementary Fig. S10) for illustration purposes. It needs to be pointed out that the melting point of nanoparticles is typically much lower than that of the bulk metal[4,25,30]. Nevertheless, we are assuming here, in agreement with our experimental observation, that key features, such as the perfect miscibility between Pt and Rh at all ratios, are maintained at the nanoscale. A segment of a revised phase diagram for the PtRh nanoparticles (shifted towards lower temperatures) is schematically shown in Fig. 6. The PtRh (3:1) nanoparticle has been shown above

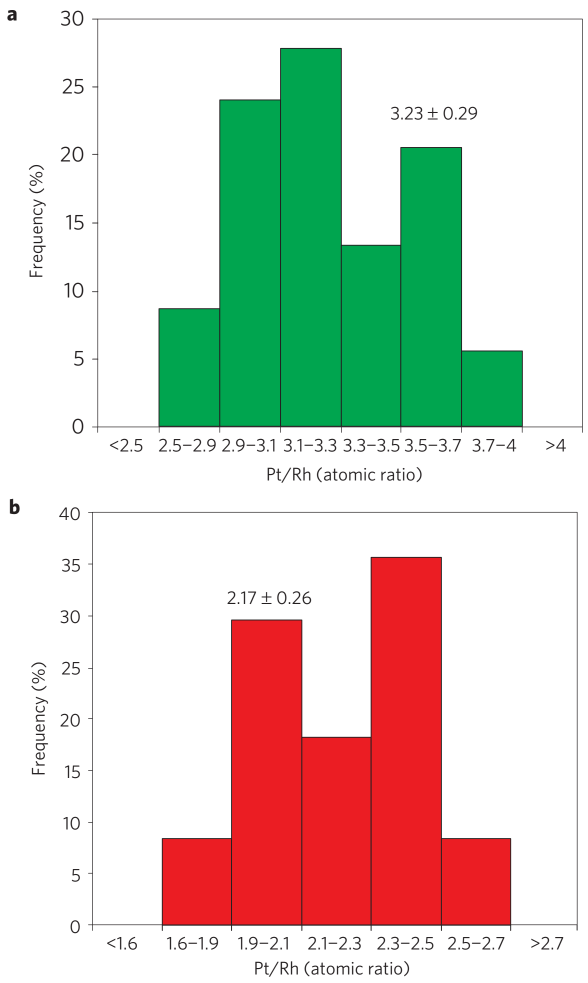

Figure 4 | Compositional statistics for PtRh nanoparticles (Pt/Rh = 3:1). **a**, Composition distribution after calcination at 600 °C. **b**, Composition distribution after calcination at 700 °C. For each set of statistics, at least 150 individual nanoparticles were selected for EDAX analysis. The numbers in the graphs show the average Pt/Rh ratio and the standard deviation of the distribution.

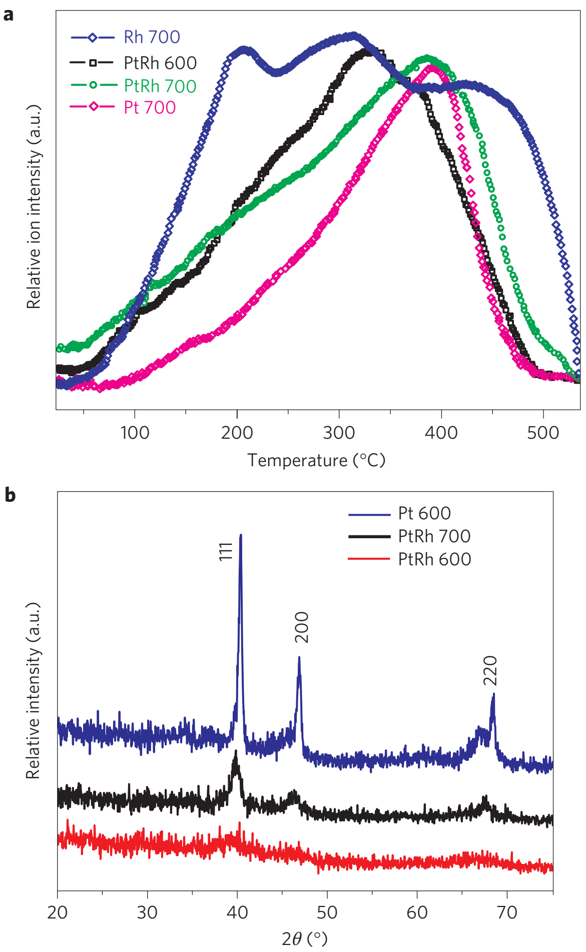

Figure 5 | CO TPD and XRD characterization of PtRh–BHA (Pt/Rh = 3:1) in comparison with monometallic Pt–BHA and Rh–BHA. a, CO TPD for PtRh–BHA calcined at 600 °C and 700 °C, respectively, in comparison with Pt–BHA (calcined at 600 °C) and Rh–BHA (calcined at 700 °C). **b**, XRD patterns for PtRh–BHA calcined at 600 °C and 700 °C, respectively, in comparison with the XRD pattern of Pt–BHA (calcined at 600 °C).

to be stable up to ~600 °C (point 1 in Fig. 6). When the sample is heated to ~700 °C, surface melting starts[25] and the nanoparticle falls into the solid–liquid zone (point 2). The lower-melting-point metal, that is, Pt, diffuses out from the PtRh nanoparticle and this highly mobile Pt phase agglomerates with Pt from other nanoparticles, and crystallizes into a larger Pt nanoparticle on cooling of the sample. The remaining PtRh nanoparticle becomes more Rh rich (point 3 in Fig. 6), as confirmed in our experiments, and hence attains a higher thermal stability. This phase separation on the individual nanoparticle level continues further with increasing temperature (points 4 and 5 in Fig. 6), similar to a distillation process: Pt bleeds from the bimetallic nanoparticle and sinters together to grow ever larger particles, and the remaining PtRh nanoparticle self-stabilizes in the mitohedrical size regime through a continuously increasing Rh content. This sacrificial behaviour is similar to a gecko's self-defence by shedding its tail.

Supplementary Fig. S11 shows that for the PtRh (3:1) nanoparticle after calcination at 850 °C, Pt nanoparticles have grown to even larger particles with sizes around 120 nm, and the Rh content in the remaining small PtRh nanoparticle has increased to 45 at%. The first investigations of other bimetallic combinations such as PtPd and PtRu demonstrate that this self-stabilization effect can be expected to be quite general: the high-melting-point metal Ru shows a similar stabilizing effect on the nanoparticles, whereas for PtPd bimetallic particles, the lower-melting-point Pd bleeds out from the bimetallic nanoparticles at lower temperature (Supplementary Fig. S12). It should finally be emphasized that the described thermal self-stabilization is not a kinetic but a purely thermodynamic effect; that is, the PtRh nanoparticles are stable at any given temperature (that is, after bleeding out the respective amount of Pt) for any extended period of time.

The described, exceptional increase in the thermal stability of nanoparticles by means of alloying has significant implications for applications such as high-temperature separation, sensing and catalysis. The last of these is illustrated here using catalytic methane combustion as an example. The light-off curve of a stream of 1 vol% CH_4 in air is shown in Fig. 7 for four different catalysts: a bimetallic PtRh–BHA catalyst (Pt/Rh = 1:1), monometallic Pt–BHA and Rh–BHA catalysts, and a pure nanostructured BHA without metal loading. All four catalysts are prepared by means of the same synthesis route and show comparable morphologies and surface areas. For pure BHA, 55% conversion of CH_4 is obtained at 650 °C, which is in good agreement with previous results[16]. Not surprisingly, the activity of the catalyst is significantly increased through the embedding of metal nanoparticles of Pt or Rh (refs 31, 32). However, for Pt–BHA, the Pt nanoparticles sinter to ~15–20 nm size at temperatures above 600 °C (refs 21, 25;

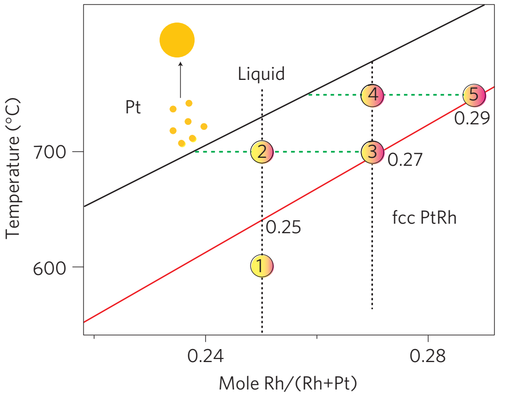

Figure 6 | Scheme for the self-stabilization mechanism of PtRh–BHA at high temperature.

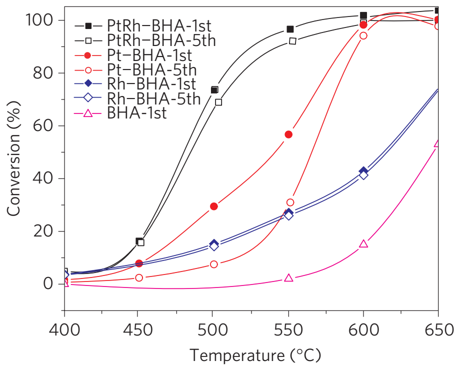

Figure 7 | Methane conversion versus reactor temperature in catalytic methane oxidation with three different BHA-based catalysts.

see also Supplementary Fig. S3), which results in a significant loss in activity after five repeated temperature cycles between room temperature and 650 °C, that is, repeated cycles of ignition and extinction of the reaction. Although Rh–BHA shows robust performance without obvious loss in catalytic activity over five continuous cycles, the intrinsic catalytic activity is much lower than that for Pt–BHA.

In contrast to the monometallic catalysts, the bimetallic PtRh–BHA sample not only shows improved activity with ignition of the CH$_4$/air stream at 450 °C and full CH$_4$ conversion around 550 °C, that is, 50–100 °C below the other samples, but, most importantly, it is stable over successive ignition–extinction cycles. Alloying Pt with Rh in the bimetallic nanocomposite PtRh–BHA catalyst hence allows combination of the high activity of Pt with the thermal stability of Rh, resulting in a single nanostructured catalyst with exceptional stability and activity.

We synthesized PtRh nanocatalysts with exceptional thermal stability by means of a microemulsion-mediated sol–gel process. The PtRh nanoparticles maintain their diameter at 4 nm at calcination temperatures of up to 850 °C. This thermal stability of these particles depends critically on the Pt/Rh ratio, with higher Rh contents leading to increased thermal stability. Phase separation is observed when the PtRh nanoparticles start to sinter: Pt bleeds out from PtRh nanoparticles and the Rh content in the remaining nanoparticle increases accordingly. This 'distillation' of the low-melting-point Pt from the PtRh nanoparticle results in a sacrificial self-stabilization of the bimetallic nanoparticles. Reactive tests in methane combustion highlight the importance of this thermal stability in catalytic applications. The described principle of thermal stabilization of bimetallic nanoparticles should be broadly applicable to the development of other multi-metallic catalysts with high reactivity and thermal stability for a variety of catalytic applications.

Methods

Synthesis of PtRh–BHA nanocatalysts. The synthesis of PtRh–BHA nanocatalysts was carried out by modifying a previously reported method[21,24]. All of the chemicals were used as received from Sigma-Aldrich without further purification. Aluminium isopropoxide (6.5 g) and barium isopropoxide (0.68 g) were dissolved in iso-propanol (125 ml) by operating on a standard Schlenk line. The solution was introduced into a prepared reverse microemulsion (15 g poly(propylene glycol)-block-poly(ethylene glycol)-block-poly(propylene glycol), 214.7 g pentanol, 65.2 g iso-octane and 12.8 g H$_2$O with H$_2$PtCl$_6$ and RhCl$_3$ dissolved inside). After a series of steps including ageing, washing, drying and calcination, BHA formed as the oxide matrix while Pt and Rh were simultaneously reduced to form the bimetallic PtRh nanoparticles. The relative amounts of H$_2$PtCl$_6$ and RhCl$_3$ were adjusted to achieve different weight loadings and atomic ratios of Pt/Rh. For each batch of synthesis, more than 2 g of PtRh–BHA with uniform morphology was obtained.

Characterizations. The particle size and distribution were analysed with TEM images using a JEOL 2000 microscope operating at 200 kV. HRTEM imaging and EDAX were carried out on a JEOL 2100 operating at 200 kV. XRD patterns were recorded on a Rigaku Dmax/rb diffractometer with CuKα radiation ($\lambda = 0.1542$ nm, 40 kV, 100 mA). Nitrogen physisorption experiments were carried out using a Micromeritics ASAP2020 surface area and porosity analyser.

CO chemisorption. The CO TPD experiment includes three consecutive steps: pretreatment, CO chemisorption and CO TPD. The sample was first oxidized in an O$_2$ atmosphere at 500 K to remove surface impurities, and then reduced in a H$_2$ stream. After cooling in He to room temperature, CO was pulse-chemisorbed to saturation. The TPD was finally carried out with a ramping rate of 10 °C min^{-1}. All of the desorbed species were monitored by a quadrupole mass spectrometer (Omnistar, Balzers).

Methane combustion experiments. The activity test for catalytic methane combustion was conducted in a fixed-bed reactor under isothermal conditions. CH$_4$ (1-vol%) and air were fed by mass flow controllers (MKS instruments, PR 4000) at a space velocity of 60,000 h^{-1}. The effluent stream was analysed by a micro-GC (Agilent 3000A) and a quadrupole mass spectrometer (Omnistar, Balzers).

Received 8 May 2009; accepted 20 October 2009;

References

1. Van Hove, M. A. From surface science to nanotechnology. *Catal. Today* **113,** 133–140 (2006).
2. Schlogl, R. & Abd Hamid, S. B. Nanocatalysis: Mature science revisited or something really new? *Angew. Chem. Int. Ed.* **43,** 1628–1637 (2004).
3. Bell, A. T. The impact of nanoscience on heterogeneous catalysis. *Science* **299,** 1688–1691 (2003).
4. Campbell, C. T., Parker, S. C. & Starr, D. E. The effect of size-dependent nanoparticle energetics on catalyst sintering. *Science* **298,** 811–814 (2002).
5. Narayanan, R. & El-Sayed, M. A. Catalysis with transition metal nanoparticles in colloidal solution: Nanoparticle shape dependence and stability. *J. Phys. Chem. B* **109,** 12663–12676 (2005).
6. Landman, U., Yoon, B., Zhang, C., Heiz, U. & Arenz, M. Factors in gold nanocatalysis: Oxidation of CO in the non-scalable size regime. *Top. Catal.* **44,** 145–158 (2007).
7. Ahmadi, T. S., Wang, Z. L., Green, T. C., Henglein, A. & El-Sayed, M. A. Shape-controlled synthesis of colloidal platinum nanoparticles. *Science* **272,** 1924–1925 (1996).
8. Rolison, D. R. Catalytic nanoarchitectures—the importance of nothing and the unimportance of periodicity. *Science* **299,** 1698–1701 (2003).
9. Häkkinen, H., Abbet, S., Sanchez, A., Heiz, U. & Landman, U. Structural, electronic, and impurity-doping effects in nanoscale chemistry: Supported gold nanoclusters. *Angew. Chem. Int. Ed.* **42,** 1297–1300 (2003).
10. Heiz, U. & Landman, U. *Nanocatalysis. Nanocatalysis* (Springer, p. preface V 2007).
11. Toshima, N. & Yonezawa, T. Bimetallic nanoparticles—novel materials for chemical and physical applications. *New J. Chem.* **22,** 1179–1201 (1998).
12. Somorjai, G. A. & Borodko, Y. G. Research in nanosciences—Great opportunity for catalysis science. *Catal. Lett.* **76,** 1–5 (2001).
13. Joo, S. H. *et al.* Thermally stable Pt/mesoporous silica core–shell nanocatalysts for high-temperature reactions. *Nature Mater.* **8,** 126–131 (2009).
14. Ott, L. S. & Finke, R. G. Transition-metal nanocluster stabilization for catalysis: A critical review of ranking methods and putative stabilizers. *Coord. Chem. Rev.* **251,** 1075–1100 (2007).
15. Narayanan, R. & El-Sayed, M. A. Effect of catalysis on the stability of metallic nanoparticles: Suzuki reaction catalyzed by PVP-palladium nanoparticles. *J. Am. Chem. Soc.* **125,** 8340–8347 (2003).

16. Zarur, A. J. & Ying, J. Y. Reverse microemulsion synthesis of nanostructured complex oxides for catalytic combustion. *Nature* **403,** 65–67 (2000).
17. Gandhi, H. S., Graham, G. W. & McCabe, R. W. Automotive exhaust catalysis. *J. Catal.* **216,** 433–442 (2003).
18. Armor, J. N. The multiple roles for catalysis in the production of H_2. *Appl. Catal. A* **176,** 159–176 (1999).
19. Ponec, V. & Bond, G. C. in *Catalysis by Metals and Alloys* (eds Delmon, B. & Yates, J. T.) (Elsevier Science, 1998).
20. Poltorak, O. M. & Boronin, V. S. Mitohedry—A new method of studying active centres in crystalline catalysts. *Russ. J. Phys. Chem.* **40,** 1436–1445 (1966).
21. Kirchhoff, M., Specht, U. & Veser, G. Engineering high-temperature stable nanocomposite materials. *Nanotechnology* **16,** S401–S408 (2005).
22. Bonnemann, H. *et al.* Nanoscale colloidal metals and alloys stabilized by solvents and surfactants—preparation and use as catalyst precursors. *J. Org. Chem.* **520,** 143–162 (1996).
23. Ponec, V. Alloy catalysts: The concepts. *Appl. Catal. A* **222,** 31–45 (2001).
24. Sanders, T., Papas, P. & Veser, G. Supported nanocomposite catalysts for high-temperature partial oxidation of methane. *Chem. Eng. J.* **142,** 122–132 (2008).
25. Wang, Z. L., Petroski, J. M., Green, T. C. & El-Sayed, M. A. Shape transformation and surface melting of cubic and tetrahedral platinum nanocrystals. *J. Phys. Chem. B* **102,** 6145–6151 (1998).
26. Palazov, A. *et al.* Adsorption and hydrogenation of ethylene, 1-hexene, and benzene and CO adsorption on Pt/Al_2O_3 and $Pt–Sn/Al_2O_3$ catalysts. *J. Catal.* **103,** 249–260 (1987).
27. Collins, D. M. & Spicer, W. E. The adsorption of CO, O_2, and H_2 on Pt: I. Thermal desorption spectroscopy studies. *Surf. Sci.* **69,** 85–113 (1977).
28. Baraldi, A. *et al.* CO adsorption and CO oxidation on Rh(100). *Appl. Surf. Sci.* **99,** 1–8 (1996).
29. Ponec, V. & Bond, G. C. in *Catalysis by Metals and Alloys* (eds Delmon, B. & Yates, J. T.) (Elsevier Science, 1998).
30. Buffat, P. & Borel, J. P. Size effect on the melting temperature of gold particles. *Phys. Rev. A* **13,** 2287–2298 (1976).
31. Schicks, J., Neumann, D., Specht, U. & Veser, G. Nanoengineered catalysts for high-temperature methane partial oxidation. *Catal. Today* **81,** 287–296 (2003).
32. Gélin, P. & Primet, M. Complete oxidation of methane at low temperature over noble metal based catalysts: A review. *Appl. Catal. B* **39,** 1–37 (2002).

Acknowledgements

This work was supported by the National Energy Technology Laboratory's on-going research under the RDS contract DE-AC26-04NT41817, by the Department of Energy—Basic Energy Science through grant DE-FG02-05ER46233 and by the National Science Foundation through grant CTS-0553365. G.V. gratefully acknowledges a CNG faculty fellowship of the University of Pittsburgh's Swanson School of Engineering. We thank Z. Liu for technical help with TEM characterizations and the Nanoscale Fabrication and Characterization Facility (NFCF) of the University of Pittsburgh for use of the electron microscopy facility.

Author contributions

A.C. carried out all experimental work, including material synthesis, characterization and catalytic tests. G.V. designed and supervised the research programme. Both contributed to data analysis, discussion and writing of the manuscript.

Additional information

The authors declare no competing financial interests. Supplementary information accompanies this paper on www.nature.com/naturematerials. Reprints and permissions information is available online at http://npg.nature.com/reprintsandpermissions. Correspondence and requests for materials should be addressed to G.V.